PHYSICAL REVIEW B **94**, 081304(R) (2016)

Polarization-dependent exciton linewidth in semiconductor quantum wells: A consequence of bosonic nature of excitons

Rohan Singh,[1,2,3,*] Takeshi Suzuki,[1,3] Travis M. Autry,[1,2] Galan Moody,[1,2,†] Mark E. Siemens,[4] and Steven T. Cundiff[1,2,3,‡]

[1]*JILA, University of Colorado & National Institute of Standards and Technology, Boulder, Colorado 80309-0440, USA*

[2]*Department of Physics, University of Colorado, Boulder, Colorado 80309-0390, USA*

[3]*Department of Physics, University of Michigan, Ann Arbor, Michigan 48105-1040, USA*

[4]*Department of Physics and Astronomy, University of Denver, Denver, Colorado 80208, USA*

(Received 28 December 2015; revised manuscript received 12 August 2016; published 29 August 2016)

The exciton coherent signal decay rate in GaAs quantum wells, as measured in four-wave mixing experiments, depends on the polarization of the excitation pulses. Using polarization-dependent two-dimensional coherent spectroscopy, we show that this behavior is due to the bosonic character of excitons. Interference between two different quantum mechanical pathways results in a smaller decay rate for cocircular and colinear polarization of the optical excitation pulses. This interference does not exist for cross-linearly polarized excitation pulses resulting in a larger decay rate. Our result shows that the bosonic nature of excitons must be considered when interpreting ultrafast spectroscopic studies of exciton dephasing in semiconductors. This behavior should be considered while interpreting results of ultrafast spectroscopy experiments involving bosonlike excitations.

DOI: 10.1103/PhysRevB.94.081304

Many-body interactions (MBIs) between excited electrons and holes, which form bound states known as excitons, are critical to understanding the optical response of semiconductor quantum wells (QWs). Experimentally, these interactions have been studied through several ultrafast spectroscopy techniques including four-wave mixing [1]. Microscopic models have been developed to understand these MBIs. One can write the light-matter interaction Hamiltonian in terms of fermionic creation and annihilation operators for electrons and holes, as in the case of semiconductor Bloch equations [2]. Alternatively, the Hamiltonian can be written in terms of bosonic operators for excitons [3–5].

While the microscopic models are critical for the theoretical understanding of exciton physics, they are computationally intensive to implement. Consequently, a few-level model of excitons is often utilized to interpret experimental results and gain a physical understanding of MBIs [6,7]. One approach starts by treating an exciton as a two-level system [8], which ignores the bosonic nature of excitons. A complimentary treatment of MBIs in excitons is inspired from their bosonic nature at low excitation densities [9–13]. This work shows that the latter approach explains some of the previous experimental results.

One of the enduring puzzles from early four-wave mixing (FWM) experiments is the dependence of signal decay rate on the polarization of the excitation pulses. It was observed that the FWM signal decays faster for cross-linearly polarized pulses than for cocircularly or colinearly polarized pulses [14–16]. A satisfactory explanation of this observation is lacking, although the contribution of disorder-mediated coupling [17], excitation-induced dephasing (EID) [18], and unbound two-exciton states [19] to the FWM signal have been proposed as explanations. Specifically, these models cannot reproduce the correct FWM signal phase, as observed in two-dimensional coherent spectroscopy (2DCS) and attributed to excitation-induced shift (EIS) [20]. The inadequacies of previous models can be partially attributed to the limitations of one-dimensional FWM experiments with respect to unraveling MBIs. We use 2DCS, which is a powerful technique to study coherent dynamics in semiconductors due to its ability to separate signals from different quantum pathways [21], to address this limitation.

Here, we show that the polarization-dependent FWM signal decay rate and phase are a direct consequence of the bosonic nature of excitons. Although these observations have been *separately* discussed previously, a self-consistent and physical explanation for both the observations has yet to be presented. Important physical insight into exciton-exciton interactions is gained by modeling excitons as interacting bosons to interpret experimental observations from 2DCS. Due to the significant reduction in computational complexity, we can fit simulation results to experimental data and quantify exciton-exciton interactions. We find that the interference between multiple pathways that contribute to the FWM signal result in different decay rates of the FWM signal and excitonic coherences. This finding is used to show that the linewidth for cross-linearly polarized excitation pulses can be *predicted* from the cocircularly polarized results using this model. While 2DCS experiments with infrared excitation pulses have revealed the bosonic nature of molecular vibrational states [22,23], the bosonic nature of QW excitons has not been previously discussed in the context of 2DCS experiments.

We describe excitons as a nearly harmonic ladder of states. Exciton-exciton interactions are introduced through anharmonic terms in the Hamiltonian [12,13]

$$H = \hbar\omega_0 \sum_{i=\pm} \hat{a}_i^\dagger \hat{a}_i + \Delta' \sum_{i=\pm} \hat{a}_i^\dagger \hat{a}_i^\dagger \hat{a}_i \hat{a}_i + \Delta_B \hat{a}_+^\dagger \hat{a}_-^\dagger \hat{a}_+ \hat{a}_-, \quad (1)$$

where $\hat{a}_i^\dagger$ and $\hat{a}_i$ are the exciton creation and annihilation operators, respectively, for spin $i = \pm 1$. The first term in

*Current address: Chemistry Division, Los Alamos National Laboratory, Los Alamos, New Mexico 87545, USA.

†Current address: National Institute of Standards and Technology, Boulder, Colorado 80305, USA.

‡cundiff@umich.edu

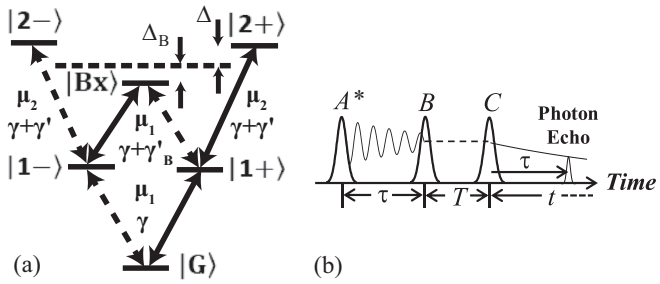

FIG. 1. (a) Energy-level scheme for excitons as anharmonic oscillators in a circular basis showing the ground $|G\rangle$, single-exciton $|1\pm\rangle$, two-exciton $|2\pm\rangle$, and biexciton $|Bx\rangle$ states. The solid and dashed arrows indicate transitions excited by light with σ_+ and σ_- polarizations, respectively. Transition dipole moments (μ_1 and μ_2) and dephasing rates (γ, $\gamma+\gamma'$, and $\gamma+\gamma'_B$) are indicated next to the arrows. Note that $\mu_2=\sqrt{2}\mu_1$. The dashed line indicates the energy of the $|2\pm\rangle$ and $|Bx\rangle$ states in the absence of interexciton interactions. The $|Bx\rangle$ state is redshifted by binding energy Δ_B and $|2\pm\rangle$ states are blueshifted by interaction energy Δ. (b) Rephasing time ordering of the pulses (A^*, B, and C) used in experiment; consecutive pulses are separated by time delays τ, and T. The signal is emitted as a photon echo during time t.

Eq. (1) is the harmonic oscillator Hamiltonian, the second term includes interaction energy Δ' between same-spin excitons, and the last term includes interaction energy Δ_B between opposite-spin excitons, which results in the biexciton state. The interaction energies are similar to phenomenological EIS [12]. The interaction energy is positive (negative) for repulsive (attractive) interaction. The anharmonic terms in Eq. (1) model the spin-dependent exchange interactions between electrons and holes as bosonic interactions between excitons. We show that this treatment brings unique physical insight to the interpretation of coherence decay dynamics of bosonlike particles.

The energy-level scheme for the Hamiltonian in Eq. (1) is shown in Fig. 1(a) with the ground $|G\rangle$, single-exciton $|1\pm\rangle$, same-spin two-exciton $|2\pm\rangle$, and biexciton $|Bx\rangle$ states. Exciton states up to the two-exciton level are shown because these are the only states that contribute to the signal in the third-order perturbation theory for the density matrix. Δ_B is assumed to be negative, indicating a bound biexciton state. EID is included by increasing the dephasing rate of $|1\pm\rangle \leftrightarrow |2\pm\rangle$ ($|1\pm\rangle \leftrightarrow |Bx\rangle$) transitions with respect to $|G\rangle \leftrightarrow |1\pm\rangle$ transitions by γ' (γ'_B). The $|G\rangle \leftrightarrow |1\pm\rangle$ and $|1\pm\rangle \leftrightarrow |2\pm\rangle$ transitions have transition dipole moments μ_1 and μ_2, respectively, related by $\mu_2=\sqrt{2}\mu_1$ [24] in the absence of the phase space filling effect, which was measured to be negligible. For convenience, we denote the energy shift of the $|2\pm\rangle$ states with respect to the unperturbed energy of two excitons as $\Delta=2\Delta'$. Although we treat the MBIs phenomenologically with the anharmonic interaction term, this model is based on the microscopic description of excitons and the interactions between them [4].

Through polarization-dependent 2DCS experiments performed on the heavy hole exciton resonance in GaAs QWs, we show that multiple quantum pathways may contribute to the signal usually attributed solely to the exciton resonance because of the bosonic nature of excitons. Consequently, the decay of the FWM signal does not necessarily correspond to the decay rate of individual transitions ($|G\rangle \leftrightarrow |1\pm\rangle$, $|1\pm\rangle \leftrightarrow |2\pm\rangle$). This fact is crucial to the dependence of the FWM signal decay rate on the polarization of excitation pulses.

2DCS is similar to a three-pulse FWM experiment with the addition of active, interferometric stabilization of the time delays and detection of the radiated FWM field as opposed to the signal intensity. The details of the experiment and the optical setup can be found elsewhere [25]. All the experiments were performed in the rephasing time ordering, shown in Fig. 1(b), where the so-called conjugated pulse A^* is incident on the sample first, followed by pulses B and C. The delay τ between pulses A^* and B was scanned, while the delay T between pulses B and C was kept constant. The signal is emitted during time t as a photon echo due to inhomogeneity in the sample. We can adjust the polarization of each of the excitation pulses and the detected signal individually. In this work we discuss results for experiments done with all the excitation pulses and signal having the same circular (cocircular), linear (colinear) polarization, or with cross-linear polarization where pulses B and C have linear polarization orthogonal to that of pulse A^* and the signal. The experiments were performed with ~200-fs-long pulses generated by a mode-locked Ti:sapphire oscillator. The delay between pulses B and C was kept constant at 300 fs to ensure well defined time ordering. On average, an exciton density of $\sim 10^{10}$ cm^{-2} per pulse per QW was excited in a four-period 10-nm-wide GaAs QW sample with 10-nm-wide $Al_{0.3}Ga_{0.7}As$ barriers. The sample was kept at a temperature of 10 K in a sample-in-vapor flow cryostat.

The result for the cocircular polarization scheme is simpler to interpret because the biexciton state does not contribute to the signal for this polarization [26]. An absolute value 2D spectrum for the cocircular polarization scheme is shown in Fig. 2(a), which has a single peak labeled P1. The negative excitation energies indicate opposite evolution of the signal phase with τ compared to its evolution during t because the conjugated pulse A^* is incident on the sample first. For a system dominated by inhomogeneous broadening, the width of the peak along the diagonal and cross-diagonal directions indicates the inhomogeneous and homogeneous linewidths, respectively [27]. Figure 2(c) shows the real part of the spectrum in Fig. 2(a); the signal phase is obtained through a complimentary pump-probe experiment [28]. The peak in Fig. 2(c) has a dispersive line shape, which has been previously attributed to EIS [20].

We calculate the FWM signal generated from the energy-level scheme shown in Fig. 1(a) by analytically solving the density matrix perturbatively up to third order in the excitation field for delta-function pulses in time. For cocircular polarization, the FWM signal is

$$S_1(\tau,t)=Ae^{-i\omega(\tau-t)}e^{-\gamma(\tau+t)}e^{-\frac{\sigma^2}{2}(\tau-t)^2}(1-e^{(i\Delta-\gamma')t}), \quad (2)$$

where A is the amplitude. ω, γ, and σ are the resonance energy, homogeneous dephasing rate, and inhomogeneous distribution width originating due to fluctuations in QW width, respectively, for the $|G\rangle \leftrightarrow |1\pm\rangle$ transition. The quantum pathways involving only the $|G\rangle \leftrightarrow |1\pm\rangle$ transitions contribute to the signal denoted by the first term in the parentheses in

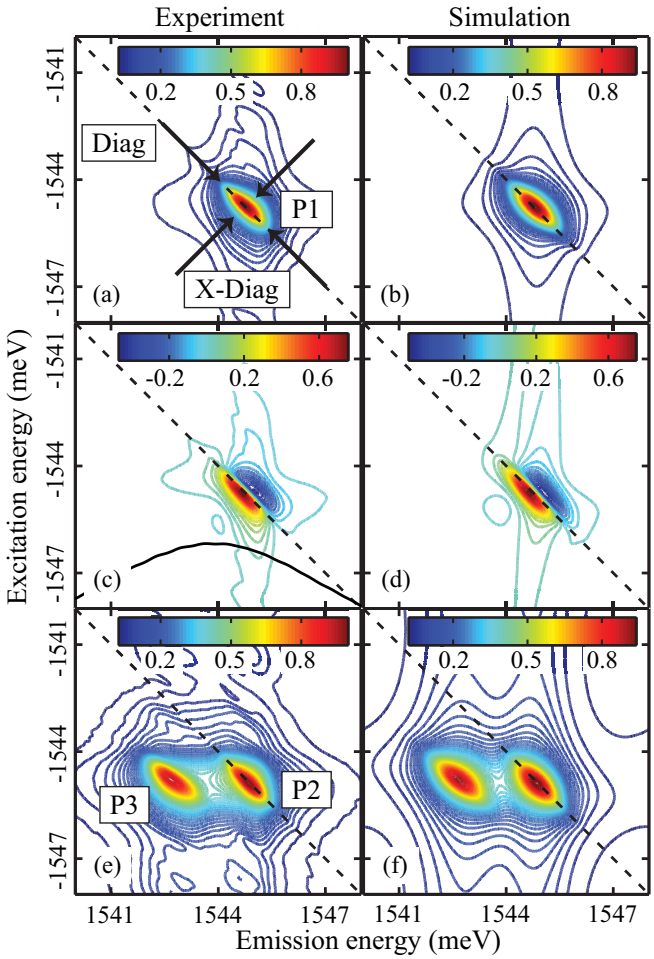

FIG. 2. Measured 2D spectra for (a) cocircular (absolute value), (c) cocircular (real part), and (e) cross-linear (absolute value) polarization scheme. The corresponding simulated spectra using best-fit parameter values are shown in (b), (d), and (f), respectively. Equal excitation and emission energy magnitudes are indicated by the dashed line in the spectra. The diagonal (Diag) and cross-diagonal (X-Diag) directions are indicated by arrows in (a). The different peaks are labeled P1, P2, and P3. The excitation spectrum is shown as the solid line in (c).

Eq. (2); the second term includes a contribution from the quantum pathways involving both $|G\rangle \leftrightarrow |1\pm\rangle$ and $|1\pm\rangle \leftrightarrow |2\pm\rangle$ transitions [29]. We assume the same inhomogeneity for both $|G\rangle \leftrightarrow |1\pm\rangle$ and $|1\pm\rangle \leftrightarrow |2\pm\rangle$ transitions. It should be noted that for $\Delta, \gamma' = 0$ both the terms in the parentheses cancel each other exactly and there is no FWM signal, as expected from a perfectly bosonic system [24]. If the above equality is not satisfied, however, this cancellation is not perfect and a nonzero FWM signal results. Specifically, for $\Delta > 0$, the real part of the signal comprises a positive and a negative peak shifted along the emission energy axis, i.e., a dispersive peak as in Fig. 2(c), for small Δ ($<\gamma$). Such a line shape is not obtained for a two-level system, which yields a single positive peak [27].

The parameters in Eq. (2) are quantified using a nonlinear fitting procedure. We simulate 2D spectra by taking a numerical Fourier transform of Eq. (2) along time delays τ and t. We then take slices through the peak of the spectrum in the real part and absolute value spectra of both the experiment and simulation. The simulated slices are then fit to the experimental ones to obtain the parameter values. The simulated absolute value and real part spectra, using the best-fit parameter values, are shown in Figs. 2(b) and 2(d), respectively. We obtain an excellent match between the measured and simulated spectra for the following parameters: $\gamma = 191 \pm 3\ \mu$eV, $\sigma = 383 \pm 2\ \mu$eV, $\Delta = 13 \pm 10\ \mu$eV, and $\gamma' = 6 \pm 6\ \mu$eV [29]. The experiment and fitting procedure was repeated five times and we report the statistical standard deviation in the parameter values as the error. As discussed earlier, the dispersive line shape in Fig. 2(c) is a consequence of $\Delta > 0$. Based on the measured values of Δ and γ', we conclude that EIS is a more dominant effect compared to EID. The measured dephasing rate γ is nearly a factor of 2 different than that obtained by fitting the diagonal and cross-diagonal slices of the absolute value spectrum to line shapes obtained by considering the exciton as a two-level system ($102 \pm 1\ \mu$eV) [27].

Figure 2(e) shows the measured absolute value 2D spectrum for the cross-linear polarization scheme. We see two distinct peaks in the spectrum, P2 and P3. The total signal for this polarization is

$$S_2(\tau,t) = e^{-i\omega(\tau-t)}e^{-\gamma(\tau+t)}\left(A_1 e^{-\frac{\sigma^2}{2}(\tau-t)^2}e^{(i\Delta-\gamma')t} - A_2 e^{i\phi}e^{-\frac{1}{2}(\sigma\tau-\sigma_B t)^2}e^{(-i\Delta_B-\gamma'_B)t}\right), \quad (3)$$

where A_1 and A_2 are the amplitudes. The term σ_B, which denotes the inhomogeneity of the $|1\pm\rangle \leftrightarrow |\mathrm{Bx}\rangle$ transitions, is included because Δ_B can, in principle, be dependent on the exciton energy, which results in $\sigma_B \neq \sigma$ [30]. A relative phase ϕ between the two terms is added phenomenologically to fit the data [29]. The other parameters are the same as in Eq. (2). The first term in Eq. (3) is the same as the second term in Eq. (2) and results in peak P2. The second term in Eq. (3) includes

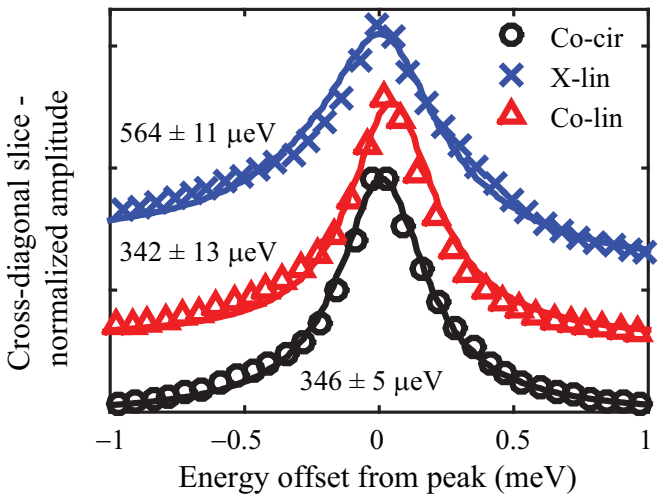

FIG. 3. The cross-diagonal slices in measured and simulated spectra are shown by markers and lines, respectively, for cocircular (Co-cir), cross-linear (X-lin), and colinear (Co-lin) polarization schemes. The slices are offset vertically for clarity. The full width at half maximum of the slices are indicated. The asymmetric line shape for cross-linear polarization is due to the wing of the biexciton peak.

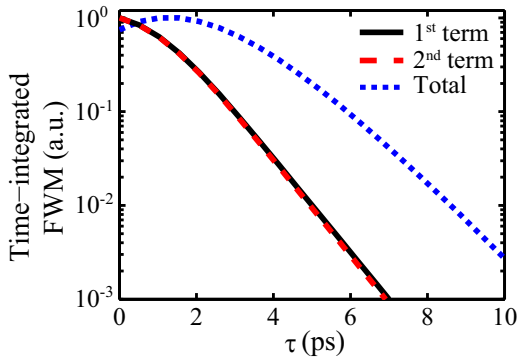

FIG. 4. Simulated time-integrated four-wave mixing (FWM) signal for the first and second terms and the total signal in Eq. (2). The signals have been rescaled to have comparable values.

contributions from quantum pathways involving $|G\rangle \leftrightarrow |1\pm\rangle$ and $|1\pm\rangle \leftrightarrow |Bx\rangle$ transitions and results in peak P3, which is redshifted along the emission energy axis relative to P2 by the biexciton binding energy Δ_B. There is no contribution to the signal from quantum pathways involving only the $|G\rangle \leftrightarrow |1\pm\rangle$ transitions due to the destructive interference of the signal from different pathways [29]. We perform a fitting procedure similar to the one discussed earlier; the resulting simulated spectrum is shown in Fig. 2(f) [29]. The parameters that define the line shape of peak P2—γ, σ, Δ, and γ'—are set to the values obtained from fitting the cocircular spectra and not varied when fitting the cross-linear spectrum.

An important observation is that peaks P1 and P2 in Figs. 2(a) and 2(e), respectively, have different widths along the cross-diagonal direction, which is apparent in the cross-diagonal slices from experimental spectra, shown in Fig. 3. In addition to cocircular and cross-linear polarization schemes, Fig. 3 also shows a cross-diagonal slice for the colinear polarization scheme (2D spectrum not shown) to compare with results of some of the earlier experiments [14–16]. We find that while the peak width along the cross-diagonal direction for cocircular and colinear polarization schemes is identical, it is greater for cross-linear polarization. Figure 3 also shows the cross-diagonal slices from the simulated spectra as lines. We emphasize that all the parameters that affect the linewidth of peak P2 were fixed during the fitting procedure for the cross-linear polarization scheme; the larger width naturally comes out of the bosonic theory.

The difference in the line shapes observed for different polarization schemes can be understood through the interference, or lack thereof, of signals from different quantum pathways that contribute to the peak appearing on the diagonal. The spectral proximity of the signal due to the different quantum pathways for cocircular polarization—including or excluding the $|1\pm\rangle \leftrightarrow |2\pm\rangle$ transitions—leads to nearly complete destructive interference at the wings of P1 in Fig. 2(a). This interference results in a total nonlinear signal with significantly narrower width compared to the individual quantum pathway contributions. To highlight this point, we plot the time-integrated FWM signal intensities for each quantum pathway [individual terms in Eq. (2)] as well as the total signal in Fig. 4. It is apparent that, independently, the FWM signal intensity from each quantum pathway is similar and decays at a fast rate (given by γ) compared to the total signal. The smaller total signal decay rate results in a narrower peak in the frequency domain. Thus, the decay rate of the total signal is significantly different than the decay rates of the individual transitions that constitute the signal. However, for the cross-linear polarization scheme, quantum pathways involving only the $|G\rangle \leftrightarrow |1\pm\rangle$ transitions do not contribute to the signal at peak P2; the aforementioned interference is absent, resulting in a much broader peak. The larger decay rate, however, reflects the true dephasing rate of the excitonic transitions. This effect is a manifestation of the bosonic character of excitons and has not been previously realized, although the scattering states of unbound two-exciton states have been considered to obtain energy-level schemes similar to the one shown in Fig. 1(a) [6,7,19,31,32]. The scattering state was either considered to have the same polarization selection rule as the biexciton state and was ignored for cocircular excitation [19,31,32] or the relation $\mu_1 = \mu_2$ was assumed [6,7], which does not give the dispersive peak observed in Fig. 2(c).

In summary, we have used 2DCS experiments to highlight the bosonic character of QW excitons and their effect on the radiated nonlinear signal. The polarization-dependent exciton linewidth is a natural consequence of this bosonic character. Exciton-exciton interactions are included in a physically intuitive and straightforward way using the model of interacting bosons. Finally, we have shown that the observed decay rate of the measured nonlinear signal can be different from the decoherence rate of individual transitions that contribute to the signal for a bosonlike system, a critical result that challenges the standard interpretation of coherent spectroscopy. In addition to providing important insight into exciton physics in QWs, these results also highlight the effects of a bosonic transition in nonlinear optics experiments. While these results are especially relevant for systems such as excitons [6,7,33] and exciton polaritons [34,35] in semiconductors, they are also important for nonlinear optical studies of bosonic quasiparticles in other systems such as surface plasmon polaritons [36], where the bosonic nature has been recently revealed [37].

The authors thank Gaël Nardin and Hebin Li for fruitful discussions. This work was primarily supported by the Chemical Sciences, Geosciences, and Energy Biosciences Division, Office of Basic Energy Science, Office of Science, US Department of Energy under Award No. DE5 FG02-02ER15346 and by the NSF under Grant No. 1125844. T.S. acknowledges support by Japan Society for the Promotion of Science (JSPS).

[1] J. Shah, *Ultrafast Spectroscopy of Semiconductors and Semiconductor Nanostructures* (Springer, Berlin, 1999).

[2] M. Lindberg and S. W. Koch, Phys. Rev. B **38**, 3342 (1988).

[3] E. Hanamura and H. Haug, Phys. Rep. **33**, 209 (1977).

[4] J.-I. Inoue, T. Brandes, and A. Shimizu, Phys. Rev. B **61**, 2863 (2000).

[5] G. Rochat, C. Ciuti, V. Savona, C. Piermarocchi, A. Quattropani, and P. Schwendimann, Phys. Rev. B **61**, 13856 (2000).
[6] G. Nardin, G. Moody, R. Singh, T. M. Autry, H. Li, F. Morier-Genoud, and S. T. Cundiff, Phys. Rev. Lett. **112**, 046402 (2014).
[7] G. Moody, I. A. Akimov, H. Li, R. Singh, D. R. Yakovlev, G. Karczewski, M. Wiater, T. Wojtowicz, M. Bayer, and S. T. Cundiff, Phys. Rev. Lett. **112**, 097401 (2014).
[8] K. Bott, O. Heller, D. Bennhardt, S. T. Cundiff, P. Thomas, E. J. Mayer, G. O. Smith, R. Eccleston, J. Kuhl, and K. Ploog, Phys. Rev. B **48**, 17418 (1993).
[9] T. Häupl, H. Nickolaus, F. Henneberger, and A. Schülzgen, Phys. Status Solidi B **194**, 219 (1996).
[10] M. Kuwata-Gonokami, S. Inouye, H. Suzuura, M. Shirane, R. Shimano, T. Someya, and H. Sakaki, Phys. Rev. Lett. **79**, 1341 (1997).
[11] M. Shirane, C. Ramkumar, Y. P. Svirko, H. Suzuura, S. Inouye, R. Shimano, T. Someya, H. Sakaki, and M. Kuwata-Gonokami, Phys. Rev. B **58**, 7978 (1998).
[12] Y. P. Svirko, M. Shirane, H. Suzuura, and M. Kuwata Gonokami, J. Phys. Soc. Jpn. **68**, 674 (1999).
[13] S. Rudin and T. L. Reinecke, Phys. Rev. B **63**, 075308 (2001).
[14] S. T. Cundiff, H. Wang, and D. G. Steel, Phys. Rev. B **46**, 7248 (1992).
[15] S. Schmitt-Rink, D. Bennhardt, V. Heuckeroth, P. Thomas, P. Haring, G. Maidorn, H. Bakker, K. Leo, D.-S. Kim, J. Shah, and K. Köhler, Phys. Rev. B **46**, 10460 (1992).
[16] H. H. Yaffe, J. P. Harbison, L. T. Florez, and Y. Prior, J. Opt. Soc. Am. B **10**, 578 (1993).
[17] D. Bennhardt, P. Thomas, R. Eccleston, E. J. Mayer, and J. Kuhl, Phys. Rev. B **47**, 13485 (1993).
[18] Y. Z. Hu, R. Binder, S. W. Koch, S. T. Cundiff, H. Wang, and D. G. Steel, Phys. Rev. B **49**, 14382 (1994).
[19] W. Langbein and J. Hvam, Phys. Status Solidi A **190**, 167 (2002).
[20] X. Li, T. Zhang, C. N. Borca, and S. T. Cundiff, Phys. Rev. Lett. **96**, 057406 (2006).
[21] S. T. Cundiff, J. Opt. Soc. Am. B **29**, A69 (2012).
[22] Y. S. Kim and R. M. Hochstrasser, Proc. Natl. Acad. Sci. USA **102**, 11185 (2005).
[23] J. Zheng, K. Kwak, J. Asbury, X. Chen, I. R. Piletic, and M. D. Fayer, Science **309**, 1338 (2005).
[24] S. Mukamel, Annu. Rev. Phys. Chem. **51**, 691 (2000).
[25] A. D. Bristow, D. Karaiskaj, X. Dai, T. Zhang, C. Carlsson, K. R. Hagen, R. Jimenez, and S. T. Cundiff, Rev. Sci. Instrum. **80**, 073108 (2009).
[26] A. D. Bristow, D. Karaiskaj, X. Dai, R. P. Mirin, and S. T. Cundiff, Phys. Rev. B **79**, 161305 (2009).
[27] M. E. Siemens, G. Moody, H. Li, A. D. Bristow, and S. T. Cundiff, Opt. Express **18**, 17699 (2010).
[28] S. M. Gallagher Faeder and D. M. Jonas, J. Phys. Chem. A **103**, 10489 (1999).
[29] See Supplemental Material at http://link.aps.org/supplemental/10.1103/PhysRevB.94.081304 for details of the calculation of the FWM signal and comparison of experimental and best-fit slices used in the fitting procedure.
[30] G. Moody, R. Singh, H. Li, I. A. Akimov, M. Bayer, D. Reuter, A. D. Wieck, A. S. Bracker, D. Gammon, and S. T. Cundiff, Phys. Rev. B **87**, 041304 (2013).
[31] E. J. Mayer, G. O. Smith, V. Heuckeroth, J. Kuhl, K. Bott, A. Schulze, T. Meier, D. Bennhardt, S. W. Koch, P. Thomas, R. Hey, and K. Ploog, Phys. Rev. B **50**, 14730(R) (1994).
[32] T. F. Albrecht, K. Bott, T. Meier, A. Schulze, M. Koch, S. T. Cundiff, J. Feldmann, W. Stolz, P. Thomas, S. W. Koch, and E. O. Göbel, Phys. Rev. B **54**, 4436 (1996).
[33] G. Moody, C. K. Dass, K. Hao, C.-H. Chen, L.-J. Li, A. Singh, K. Tran, G. Clark, X. Xu, G. Berghauser, E. Malic, A. Knorr, and X. Li, Nat. Commun. **6**, 8315 (2015).
[34] B. L. Wilmer, F. Passmann, M. Gehl, G. Khitrova, and A. D. Bristow, Phys. Rev. B **91**, 201304 (2015).
[35] N. Takemura, S. Trebaol, M. D. Anderson, V. Kohnle, Y. Léger, D. Y. Oberli, M. T. Portella-Oberli, and B. Deveaud, Phys. Rev. B **92**, 125415 (2015).
[36] S. Palomba and L. Novotny, Phys. Rev. Lett. **101**, 056802 (2008).
[37] G. Di Martino, Y. Sonnefraud, M. S. Tame, S. Kéna Cohen, F. Dieleman, Ş. K. Özdemir, M. S. Kim, and S. A. Maier, Phys. Rev. Appl. **1**, 034004 (2014).